

Exoplanet Clouds

Christiane Helling

Centre for Exoplanet Science, University of St Andrews,
St Andrews KY16 9SS, UK;
email: ch80@st-andrews.ac.uk

Annual Review of Earth and Planetary
Sciences 2018. 47:1–26

[https://doi.org/10.1146/\(\(please add article doi\)\)](https://doi.org/10.1146/((please add article doi)))

Copyright © 2018 by Annual Reviews.
All rights reserved

Keywords

exoplanets, clouds, atmospheres, complex, modelling, condensation, clusters, weather

Abstract

Clouds also form in atmospheres of planets that orbit other stars than our Sun, in so-called extrasolar planets or exoplanets. Exoplanet atmospheres can be chemically extremely rich. Exoplanet clouds are therefor made of a mix of materials that changes throughout the atmosphere. They affect the atmospheres through element depletion and through absorption and scattering, hence, they have a profound impact on the atmosphere’s energy budget. While astronomical observations point us to the presence of extrasolar clouds and make first suggestions on particle sizes and material compositions, we require fundamental and complex modelling work to merge the individual observations into a coherent picture. Part of this is to develop an understanding for cloud formation in non-terrestrial environments.

Contents

1. INTRODUCTION	2
2. Exoplanet cloud observations	2
3. How clouds form on exoplanets	5
3.1. Cloud formation processes	5
4. A generic case study for exoplanet clouds in 1D	10
4.1. Thoughts on model completeness	13
4.2. Summary of take-away points about clouds in exoplanet atmospheres	14
5. Exoplanet element abundances and mineralogic ratios	14
5.1. Summary of take-away points on element abundances in exoplanet atmospheres	16
6. Cloudy weathers on extrasolar planets	18
6.1. Lightning on exoplanet and the extrasolar global electric circuit	20
6.2. Summary of take-away points in 3D extrasolar clouds	21
7. Future issues	21

1. INTRODUCTION

By June 2018, 3796 extrasolar planet were known to exist. These planets are residing in 2840 planetary systems of which 632 contain multiple planets (Exoplanet.eu). If both mass and radius are known, a mean density can be derived which provides us a first idea about if the planet is made of light elements like hydrogen and helium, or if it contains a large fraction of water, rock and/or iron. The planetary composition is determined by the planet's formation process and the material that is accreted onto the planet from the planetary disk. Planets that form very close to their host star will predominantly accrete materials that contain large amounts of Mg/Si/Fe/O, hence, they are termed 'rocky planets'. Planets that form at the outskirts of the planet forming disks, where temperatures are low enough that ices of all sorts (H₂O ice, CO ice, CH₄ ice) form, will consequently contain carbon, hydrogen and considerable amounts of oxygen but also large amounts of Mg/Si/Fe as part of their cores. The planetary atmosphere forms through gas accretion and, later, mainly through outgassing (incl. volcanism) of the accreted disk material. We may therefore expect to find fingerprints of the planet formation process by studying its atmosphere. However, our enthusiasm has been challenged by the discovery that many, if not all, extrasolar planets will be enshrouded by clouds. This realisation will have a considerable impact on target selection for upcoming space missions (e.g., James-Webb Space Telescope (JWST) that aims to characterise exoplanet atmospheres in the infrared spectral range) for which planets were expected to be entirely cloud-free. Only the hottest exoplanets that are closest to their host star may expose a clear dayside and some a lava-like surface.

2. Exoplanet cloud observations

Clouds on exoplanets were postulated as the reason for missing molecular or atomic absorption features expected to be detected in the optical and near-IR spectra as obtained from from space- (e.g. Hubble-Space Telescope (HST) which took the first picture of an exoplanet in the optical spectral range) and ground-based (e.g with the optical Very Large Telescope composed of four 8.2 m telescopes that can be combined into an interferometer) observations. Brown Dwarfs were the first class of objects discover to have extensive at-

atmospheric clouds. Brown Dwarfs undergo different formation processes than planets. They form as stars (hence, ignite some nuclear fusion which planets don't) and not as part of a stellar accretion disk. Clouds have a distinct impact on the atmospheric profiles of Brown Dwarfs and planets. In order to reflect this, different classes of Brown Dwarfs were suggested for classification purposes: L dwarfs (clouds in observable atmosphere) and T dwarfs (clouds affect atmosphere but are below observable atmosphere). More recently, the Y dwarfs were added. These are Brown dwarfs, hence stellar objects, that are most similar to planets regarding their very low global temperatures ($T_{\text{eff}} < 200\text{K}$; T_{eff} is the effective temperature and it measures the total radiation output of an object). Since their discovery, Brown Dwarfs have been studied as analogues of extrasolar planets also with respect to their atmospheric processes. This is supported particularly by the overlapping mass regimes, but also by the location of very low gravity Brown Dwarfs and free-floating planets in the colour-magnitude (J-K) diagram (Charnay et al. 2018). Brown Dwarfs further exhibit rotating, banded cloud structure similar to what is seen on Jupiter in optical wavelengths. Their atmospheric dynamics resembles best the Neptunian atmosphere (Apai et al. 2017). Given such similarity, we expect to find vertically (and horizontally) extended cloud structures in exoplanets, similar to what has already been spectroscopically demonstrated for Brown Dwarfs (e.g., Apai et al. 2013). The first extrasolar planet for which an extensive cloud layer was derived from observations is the $1.15 M_{\text{Jup}}$ mass giant gas planet HD 189733b¹ orbiting a K-dwarf star in 2.2 days. Pont et al. (2013) present a transmission spectrum (i.e. observations of the planet transiting in front of the star at different wavelengths) ranging from the UV to the near-IR and find that it is dominated by starlight being scattered by small particles in the planet's upper atmosphere. A flat optical exoplanet spectrum without any molecular absorption was also obtained by persevering HST observations of the super-Earth GJ1214b (Kreidberg et al. 2014). Similarly, the small rocky exoplanet GJ 1132b² ($1.2R_{\text{Earth}}$, $1.6M_{\text{Earth}}$) that orbits a M-dwarf shows a $0.7\mu\text{m}$ - $1.04\mu\text{m}$ spectrum with no gas absorption features (Diamond-Lowe et al. 2018). This could be caused by a cloud-free atmosphere that is extremely metal rich ($10\times$ solar; i.e. enriched in elements heavier than hydrogen) which cannot be $\text{H}_2\text{O}/\text{H}_2$ -dominated. The only other options are that the rocky planet has lost its atmosphere, for example through the high-energy radiation impact from its host star, or that the planet is enshrouded in vertically and globally extended clouds.

The method that is most widely applied to analyse the chemical composition of extrasolar planets, at the time of writing, is transmission spectroscopy. A transmission spectrum is obtained by observing the planet transiting in front of a star at different wavelengths and then measuring the magnitude of the transit depth in the resulting light curve. It records the opacity of the atmosphere at different wavelengths. To account for clouds, in the literature such observations are fitted by presetting the material composition and by assuming a constant size of cloud particles in the optical, and alternatively a second size for larger wavelengths. However, exoplanet cloud particles are neither made of just one material because of their chemically rich atmospheres, nor do they occur with just one size. Instead, exoplanet clouds are made of a rich mix of materials in atmospheres that cover a

¹HD refers to stars which have been catalogued in the Henry Draper Catalogue. The small letter behind the catalogue number (189733) indicates that HD 189733b is a planet orbiting the star HD 189733.

²GJ refers to stars which are catalogued in the Gliese Catalogue of Nearby Stars. The small letter behind the catalogue number indicates that it is a planet orbiting the star GJ 1132.

wide range of temperatures. Most recently, high-dispersion spectroscopy was developed to analyse the atmospheric gas also for non-transiting planets (Snellen et al. 2013).

Comprehensively understanding exoplanet atmospheres is very much linked to the understanding of the cloud formation mechanisms. Clouds exert strong feedbacks on an exoplanet atmosphere causing visible changes to the observed spectrum:

- a) Cloud particles have a far larger opacity (absorption + scattering) than the atmospheric gas, hence, they absorb and re-emit more photons. This results in a strong heating of the atmosphere below the clouds (greenhouse effect, backwarming) but also in a redistribution of the incoming stellar flux through hydrodynamical processes. Clouds block our view into the underlying atmosphere such that telescopes can only access the atmospheric layers above them.
- b) During their formation, the cloud particles consume elements such that molecules and atoms containing those elements (e.g. Si/SiO, Mg/MgOH, Ti/TiO₂, O/H₂O) will appear less abundant. This effect is best observable for less abundant elements like Ti, V or Al showing less than expected absorption in e.g. TiO. Any observational element abundance determination needs therefore to be conducted with great care as only the atmospheric part above an optically thick cloud layer can be observed.

Astronomical observations provide us with exciting discoveries, but with only limited information about any of the exoplanets. We may know the planetary mass and radius, or only one of the two, the radius ratio planet-to-star at specific wavelengths (transmission spectrum), the integrated thermal flux or the albedo. To merge these pieces of observations into a coherent picture, chemically and physically consistent models that apply detailed knowledge of the cloud formation processes, the gas chemistry, energy transport through radiative and/or convection are required. From Earth we know that the diversity of cloud structures (size, form) is indicative of the local atmospheric conditions and their history. Thus, the aim of this review is to discuss cloud formation as a necessary part of a complex modelling approach, which is the base for our understanding of the plethora of exoplanet atmosphere observations that will come from space telescopes like CHEOPS³, TESS⁴, JWST⁵, PLATO⁶, ARIEL⁷, WFIRST⁸, LUVOIR⁹ and also from high-precision ground-based instruments like FORS2¹⁰, ESPRESSO¹¹ and CARMENES¹² at the VLT¹³.

³CHEOPS stands for CHaracterising ExOPlanets Satellite; <http://cheops.unibe.ch>

⁴TESS stands for Transiting Exoplanet Survey Satellite; <https://www.nasa.gov/tess-transiting-exoplanet-survey-satellite>

⁵JWST stands for James-Webb Space Telescope; <https://www.jwst.nasa.gov>

⁶PLATO stands for PLANetary Transits and Oscillations of stars and is a space telescope; <http://sci.esa.int/plato/>

⁷ARIEL stands for Atmospheric Remote-sensing Exoplanet Large-survey and is a space mission; <https://ariel-spacemission.eu>

⁸Wide Field Infrared Survey Telescope; <https://wfirst.gsfc.nasa.gov>

⁹Large UV/Optical/IR Surveyor; <https://asd.gsfc.nasa.gov/luvoir/>

¹⁰FORS2 stands for FOcal Reducer/low dispersion Spectrograph 2; <https://www.eso.org/sci/facilities/paranal/instruments/fors/overview.html>

¹¹ESPRESSO stands for chelle SPectrograph for Rocky Exoplanets and Stable Spectroscopic Observations; <https://www.eso.org/sci/facilities/paranal/instruments/espresso.html>

¹²CARMENES stands for Calar Alto high-Resolution search for M dwarfs with Exoearths with Near-infrared and optical Échelle Spectrographs; <https://carmenes.caha.es/ext/instrument/index.html>

¹³VLT stands for Very Large Telescope; <https://www.eso.org/public/teles-instr/>

3. How clouds form on exoplanets

The formation of clouds occurs through a sequence of chemical and physical processes that are determined by the local atmospheric gas temperature, pressure and chemical composition. The gas composition is determined by the number and abundance of elements (H, He, Si, Fe, Mg, O, C etc.) available. This initial amount of elements is determined through stellar (nuclear synthesis) and planetary (pebble accretion, outgassing, atmosphere loss) evolutionary processes. The most abundant molecules in a solar-composition, hydrogen-rich planetary atmosphere are H_2 , H_2O , CO , CH_4 , N_2 , NH_3 followed by SiO , H_2S , $\text{Fe}(\text{OH})_2$, $\text{Mg}(\text{OH})_2$, and less abundant molecules like AlO_2H , SiS , TiO_2 and others (Woitke et al. 2017) will contribute to the cloud formation processes. These atoms, molecules and potentially ions are the starting point of the cloud formation. Their relative abundances change if the relative number of the individual elements (O, C, Si, Mg, Fe, Ca, Al etc.) changes and the thermodynamic condition of the gas changes. These processes form a closed feedback circle. Hotter atmospheres, like the day-side of the rocky planet CoRoT-7b (Mahapatra et al. 2017) and of ultra-hot Jupiters (Parmentier et al. 2018; Lothringer et al. 2018), will contain more atomic and ionic species, cooler atmospheres will be dominated by molecules. This effect is well-known from stellar atmospheres (e.g. Gustafsson et al. 2008). For example, the hydrogen ion, H^+ , is an important opacity in hot Jupiters like WASP-18b because of their very high days-side temperatures (Arcangeli et al. 2018). Such high gas temperatures do not permit cloud formation. Various modelling approaches for considering clouds as part of atmospheric modelling have been developed and were compared in Helling et al. (2008a) and a summarising update is provided by Charnay et al. (2018). All but one of the approaches invokes phase-equilibrium (thermal equilibrium). In the following, we will focus on the cloud formation processes which require the deviation from phase-equilibrium to enable the actual formation to occur.

3.1. Cloud formation processes

Clouds form through and are influenced by a sequence of processes that are summarised in Figure 1. These processes are universal and will therefore occur whenever the local conditions for temperature, gas density and wind speed are favorable. Cloud formation is seeded by the emergence of condensation nuclei (**nucleation**, Sect. 3.1.1) onto which all thermally stable materials grow through gas-surface reactions (**bulk growth**, Sect. 3.1.2). As the atmosphere is gravitationally bound by the mass of the planet, the cloud particles will gravitationally settle (**gravitational settling**, rain out). As they fall (gravitational settling, Sect. 3.1.3), they will encounter different temperatures and gas densities which cause the material composition of the cloud particles to change because of changing thermal stability. The cloud particles continue to grow until the temperatures are too high and the materials begin to evaporate. Thermal stability increases if the local gas pressure increases for a given temperature. The condensation and evaporation processes change the local element abundances because participating elements are depleted. This, in turn, changes the species that continue the bulk growth process. The depletion of oxygen, for example, will lead to an increase of the local carbon-to-oxygen ratio (C/O). In order for a cloud layer to persist, element replenishment (Sect. 3.1.3) mechanisms in form of convection and/or diffusion must be active. The vertical, geometric extension of a cloud is determined by the presence of

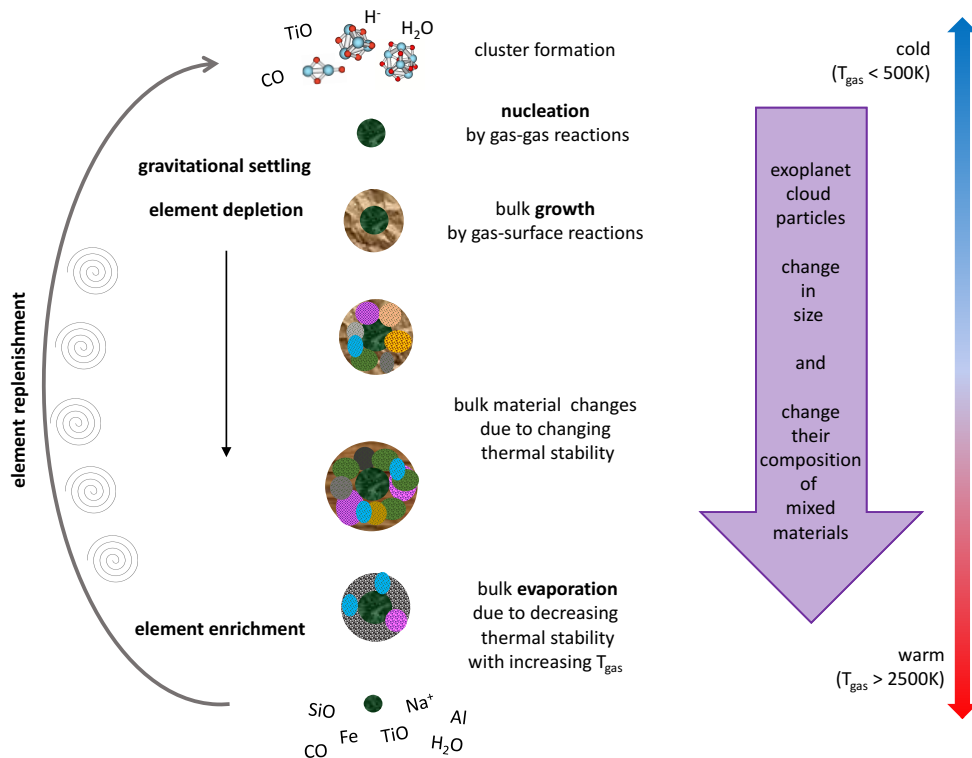


Figure 1

Cloud formation processes leading to cloud particles made of a mix of material that changes with height. Cloud formation in extrasolar planets starts from a chemically very rich gas (including e.g. CO , SiO , CaH , H_2O , TiO_2 , $\text{Mg}(\text{OH})_2$). If the temperature is low enough, big molecular structures (so-called clusters) begin to form and grow to condensation nuclei (**nucleation**). Subsequently, many materials condense onto these seed particles and they **grow** to macroscopic μm -sized cloud particles. The cloud particles fall into the atmosphere (**gravitational settling**) where they may change their material composition and sizes completely, until they **evaporate**. The condensation processes **deplete** the atmosphere of elements, and the evaporation process will **enrich** the atmosphere. A stationary cloud forms of an efficient **element replenishment** mechanism is active. Courtesy to David Gobrecht for the $(\text{Al}_2\text{O}_3)_{1,2,3}$ cluster structure.

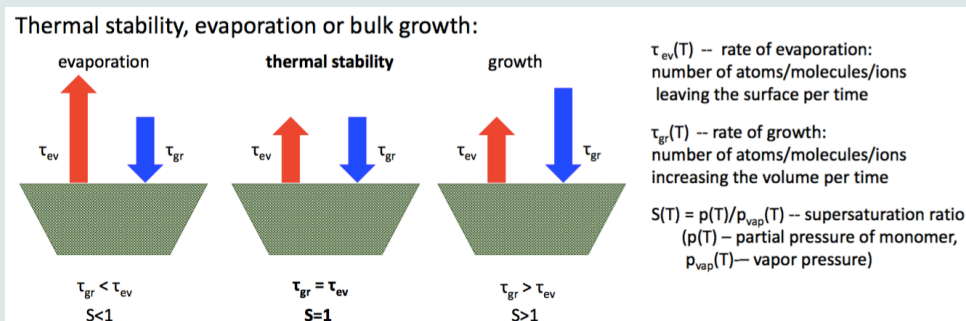
condensation nuclei (or their formation) at the upper boundary and by the thermal stability at the lower boundary.

3.1.1. Nucleation / seed formation. On Earth, most of the cloud particle (aerosols, droplets) form inside the troposphere where condensation seed particles (cloud condensation nuclei – CCN) are available from, for example, sand storms, ocean spray, fires, combustion and volcano eruptions. Without the presence of a condensation seed, spontaneous water condensation from the gas phase requires a supersaturation of 800% on Earth which has not been observed. This statement is well-accepted by scholars in different disciplines (me-

teorology, earth and environmental science, astronomy) but it poses a conundrum. The measurement of the supersaturation in the Earth atmosphere can not distinguish between the two following cases: i) The water has condensed onto condensation seeds. ii) The thermodynamic conditions are inappropriate for water nucleation (spontaneous condensation) to occur. The conundrum is that in both cases the atmospheric gas will be at or near the phase-equilibrium level and therefore, the gas will not be supersaturated at all (see gray box). Both cases lead to the conclusion that water condensation on Earth can not occur directly from the gas phase. For extrasolar planets, it is impossible to measure rates for condensation seed production (like through volcano outbreaks) in situ. It is therefore necessary for Earth and for extrasolar planets alike to seek out more fundamental approaches that enable us to predict how many condensation seeds form from the gas phase to start with. Similar challenges are known from the formation of clouds in the Earth's mesosphere (noctilucent/mesospheric clouds), where evaporating meteorites play their role in forming meteoritic smoke particles onto which H₂O ice condenses (Plane et al. 2018), but also from the occurrence of nucleation bursts in Earth's convective boundary layers (Hellmuth 2006). Similar challenges arise for other solar system planets. For example, Martian mesospheric clouds have been identified, too, but are predominantly of CO₂ ice (Määttä et al. 2010).

Supersaturation and supercooling

The concept of *thermal stability* of a material (e.g. TiO₂[s], SiO[s]) is defined for a planar, infinitely extended surface and it occurs if the *supersaturation* ratio $S(T)=1$. The same concept is applied to non-planar surfaces when considering clouds. Thermal stability represents a state of equilibrium because the rate of evaporation, τ_{ev} , equals the rate of growth, τ_{gr} , as shown in the figure below. However, growth and evaporation are non-equilibrium states as $\tau_{ev} \neq \tau_{gr}$. The formation of condensation seeds from the gas phase requires a considerable supersaturation of the participating gas because the evaporation rate increases with decreasing cluster size for any given temperature (Goeres 1996). The necessary supersaturation ($S \gg 1$) requires a considerably lower temperature (*supercooling*: $T_{gas}(S \gg 1) \ll T_{gas}(S=1)$) than suggested by thermal stability arguments.



The formation of seed particles is a chain (or a network) of chemical reactions that lead to an increasing complexity with each step: Larger and larger molecules form that eventually are of the size of clusters. Each of the reaction steps leads to the formation of the next more complex cluster, e.g. $TiO_2 + TiO_2 \rightarrow (TiO_2)_2 + TiO_2 \rightarrow (TiO_2)_3 + TiO_2 \rightarrow \dots$

$\rightarrow (\text{TiO}_2)_{100} \dots \rightarrow \text{TiO}_2[\text{s}]$ (, [s]' stands for solid). The study of TiO_2 -cluster formation suggests a chemical path where the same molecule (monomer TiO_2) is added during each reaction step (Jeong et al. 2000). Other species may not form that easily from the gas phase as their monomers are not available as gas species. Examples are silicates like Mg_2SiO_4 , or metal oxides like Al_2O_3 . $(\text{Al}_2\text{O}_3)_n$ clusters have been observed in extended gaseous envelopes of very cool, giants stars (Decin et al. (2017) but the formation mechanisms is as of yet uncertain. A further challenge is that monomers may exist in many different geometrical configurations (isomers) that are equally favorable (e.g. MgSiO_3 , Patzer et al. 2002). Metal clusters have also been studied but the example of iron is discouraging as the $(\text{Fe})_2$ -cluster appears to be very unstable such that the cluster growth chain of increasing complexity is interrupted already at small cluster sizes. The CLOUD (Cosmics Leaving Outdoor Droplets) experiment at CERN (the European Organization for Nuclear Research) has demonstrated that external radiation like through high-energy particles from cosmic rays can support the formation of condensation nuclei (Dunne et al. 2016). Stellar radiation (Rodríguez-Barrera et al. 2018) and cosmic rays (Rimmer et al. 2014) ionise the high-altitude atmospheric regions such that nucleation processes may involve complex ions in exoplanets atmosphere at high altitudes. But the locally very low gas densities in the upper atmospheres may render the whole processes inefficient for cloud or haze formation. The most studied nucleation species is carbon which is only relevant for exoplanets if the atmospheric gas is strongly oxygen depleted or primordially carbon rich (Helling et al. 2014).

3.1.2. Bulk growth/evaporation: mixed-material cloud particles with a non-homogeneous size distribution. The chemical diversity of exoplanet atmospheres allows for plenty of materials being thermally stable almost simultaneously. Once condensation seeds have been formed, these materials condense simultaneously onto the seed's surface. Condensation of materials on existing surfaces only requires a moderate supersaturation and is therefore far easier occurring than the nucleation processes addressed in Sect. 3.1.1. Exoplanet atmospheres are expected to be predominantly oxygen rich because all carbon is bound either in CO or in CH_4 but CO_2 for hydrogen-poor gases. However, small rocky planets may have lost their atmosphere or large fractions of their atmospheric mass. Hydrogen, as the lightest element, would be the first element to escape leaving behind a hydrogen-poor atmosphere with an increased mean molecular weight ($\mu = \sum n_i m_i / \sum n_i$, n_i [cm^{-3}] - number density of gas species i , m_i [g] - mass of gas species i). Materials that form the volume (and mass) bulk of the cloud particles in hydrogen-poor (rocky) planets and hot, giant gas planets will therefore include silicates (e.g. $\text{Mg}_2\text{SiO}_4[\text{s}]$, $\text{MgSiO}_3[\text{s}]$, $\text{SiO}_2[\text{s}]$, $\text{Fe}_2\text{SiO}_4[\text{s}]$), metal oxides (e.g. $\text{TiO}_2[\text{s}]$, $\text{Al}_2\text{O}_3[\text{s}]$, $\text{MgO}[\text{s}]$, $\text{FeO}[\text{s}]$) and others (e.g. $\text{Fe}[\text{s}]$, $\text{CaTiO}_3[\text{s}]$, $\text{FeS}[\text{s}]$). If Mg/Fe/Si/O are the most abundant species, as known to be the case for the Sun, then these silicates will form the matrix of the cloud particles that has mixed-in impurities from materials involving less abundant elements (e.g. Ti and Al). For colder exoplanets (Earth-like, mini-Neptune), additional species may condense ($\text{H}_2\text{O}[\text{l}]$, $\text{NH}_3[\text{l}]$, $\text{FeS}[\text{s}]$). While the aforementioned solids remain thermally stable also at low temperatures, and therefore keep condensing, they may rearrange into more complex materials like phyllosilicates as suggested by thermal equilibrium studies (e.g. $\text{Mg}_2\text{SiO}_4[\text{s}] \rightarrow \text{Mg}_3\text{Si}_2\text{O}_9\text{H}_4[\text{s}]$, $\text{NaAlSi}_3\text{O}_8[\text{s}] \rightarrow \text{NaMg}_3\text{AlSi}_3\text{O}_{12}\text{H}_2$). The exact details are extremely sensitive to the treatment of the element abundances in such equilibrium considerations. A more robust result is that H_2O and NH_3 condense at $T < 250\text{K}$, and that other species like $\text{NaCl}[\text{s}]$, $\text{FeS}[\text{s}]$, $\text{Fe}[\text{s}]$, $\text{Ni}[\text{s}]$ will appear as impurities in such icy cloud particles in exoplanet atmospheres. Woitke et al.

(2017) have presented the most stable condensation phases depending on local temperature and pressure (phase diagrams) for all elements composing the solar element abundance set including the effect of element depletion through the condensation process. Such phase diagrams, however, do not allow to determine the cloud particles sizes and a kinetic approach is required for the actual calculations of the growth (and evaporation) rates for each of the materials involved. Knowledge about the individual reaction is required but laboratory data are only sparsely available. For example, the formation of $\text{Mg}_2\text{SiO}_4[\text{s}]$ alone can involve 11 gas-surface reactions requiring Mg, Si, MgOH , $\text{Mg}(\text{OH})_2$, MgS , MgH , MgN , SiO , SiS , and H_2O from the gas phase. One efficient method to include all these details in order to calculate cloud particle properties (nucleation rates, material compositions, column densities, particle sizes) is a moment method as described in Helling & Fomins (2013). Another method involves the binning of the particle size distribution (Krüger & Sedlmayr 1997; Powell et al. 2018). Both methods were also developed for dust formation modelling in AGB-stars envelopes.

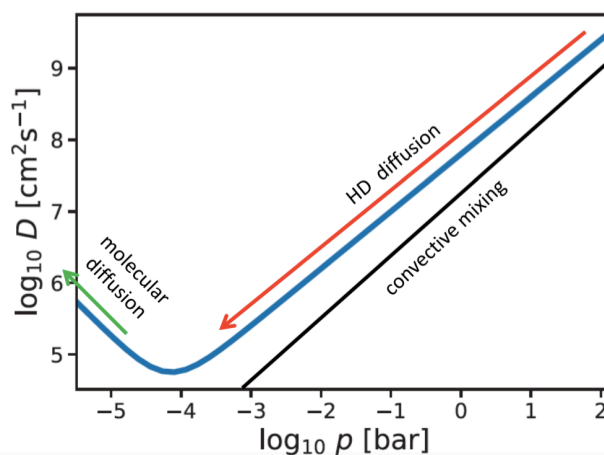


Figure 2

Element replenishment in exoplanet atmospheres can proceed through diffusive (blue line) and convective mixing (black line). Both decay with decreasing pressure, p [bar], but diffusion will pick up again at the lowest pressures (green arrow) through molecular processes becoming more important than large-scale hydrodynamical processes (red arrow).

3.1.3. Gravitational settling and element replenishment. Cloud particles will move through the atmospheres with the gas if the frictional coupling (drag) is strong, i.e., they would be swept along with the wind. The cloud particles decouple from the gas if the drag force is too small, hence, if the particles are too heavy or the gas density is too low. This leads to the cloud particles falling (gravitational settling) through the atmosphere with a speed that is determined by their radius and material density, but also by the surrounding gas density (Woitke & Helling 2003). Rain occurs if the cloud particles fall faster than the growth processes can occur. In this case, their sizes remain constant until they possibly evaporate. As the cloud particles move through the atmosphere, they deplete the gas phase locally if they grow and they enrich the local gas phase if they evaporate. Therefore, in order for a largely

continuous cloud coverage to be present in an atmosphere, the gas needs to be replenished through hydrodynamical transport processes. Such hydrodynamic motions include small-scale advection and large scale convection, but gas replenishment can also proceed via the much slower diffusion processes. The critical difference here is that advection and convection transport a bulk of gas (fluid) with the hydrodynamic (wind) velocity over a considerable distances (e.g. day-night side equatorial jets, Showman et al. 2008; Dobbs-Dixon & Agol 2013; Mayne et al. 2014), and that diffusion differentiates between the different gas species as it depends on their masses (e.g. Moses et al. 2000). Figure 2 demonstrates that the diffusion reaches a minimum when the large-scale motions become inefficient but picks up again at lower densities due to the small-scale molecular diffusion processes. A purely convective representation would drop in efficiency with increasing distance from the convectively active regime. The bulk transport of gases as well as diffusive transport is part of the solution of 3D hydrodynamic simulations. The challenge is to provide a workable representation of element replenishment for 1D atmosphere simulations which are far more efficient, in particular if cloud formation, gas-phase chemistry and radiative transfer are a coupled part of the complex model solution. So far, numerical experiments testing diffusive material transport have been conducted for cloud-free 3D simulations only (Parmentier et al. 2013; Zhang & Showman 2018). While being limited in their chemical completeness, each numerical experiment is further limited by its spatial (and time) resolution. This becomes critical for processes predominantly acting on similar and smaller scales and it is known as ‘turbulent closure problem’. Large efforts are going into representing such sub-grid processes in Earth weather modelling (e.g. Smith 1990) and in engineering (e.g. Glawe et al. 2015). Turbulent, small-scale fluctuations will extent the cloud formation regime for exoplanets and amplifies the intermittency of the cloud coverage (Helling et al. 2004), but turbulence also facilitate cloud particle charging in exoplanet atmospheres (Helling et al. 2011, 2016c).

4. A generic case study for exoplanet clouds in 1D

Cloud formation is determined by the local thermodynamic state (gas temperature and gas pressure) of the atmospheric gas. The thermodynamic state will be affected by the planet size and the external radiation from the host star (lava planets vs. giant gas planets) or the interplanetary medium (‘directly imaged planets’, i.e. planets with a large orbital distance from their host star), by the interaction between the atmosphere and the crust (rocky planets), and by the evolutionary state (young vs old) of the planet itself. Because of the large diversity of exoplanets, it is desirable to develop a fundamental understanding about their atmospheres and about exoplanet clouds. We therefore choose a generic case to discuss predictive results. Our example represents a moderately warm giant gas planet (directly imaged and/or self-luminous young planet) with effective temperature $T_{\text{eff}}=1800\text{K}$, surface gravity $\log(g)=3.0$, an initial set of solar element abundances (i.e. the number of elements of one kind contained in all gas species, e.g. Si in SiO , SiH , SiO_2 , MgSiO_3 , SiS etc., or Fe in Fe , FeO , FeS , FeSiO_3 etc.) and with enough distance from its host star that stellar irradiation does not matter. The results are obtained from considering the formation of three nucleation species simultaneously (TiO_2 , SiO , C), and the formation of 15 bulk materials (listed in Fig.3) that form from 9 elements (Mg, Si, Ti, O, Fe, Al, Ca, S, C) by 126 surface reactions. The approach is based on Helling et al. (2008b) and follows the principles described in Sect. 3. Figure 3 presents the exoplanet cloud results for a set of characteristic properties :

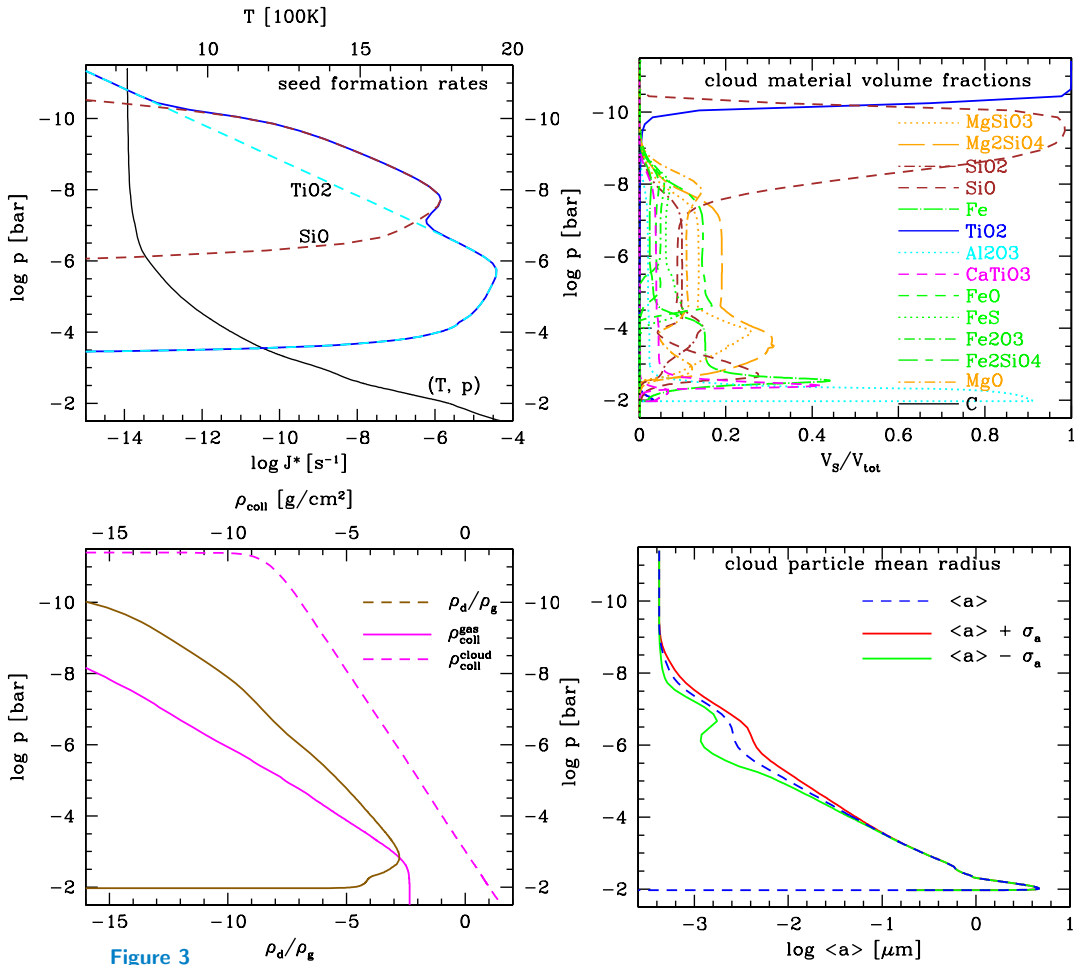


Figure 3

Characteristic cloud properties in a hot exoplanet ($T_{\text{eff}}=1800\text{K}$, $\log(g)=3.0$, solar element abundances; (temperature T [K], pressure p [bar])-profile – black solid line in top left). The nucleation rate (J^* [s⁻¹], top left) determines the number of cloud particles unless transport processes sweep up condensation seeds from elsewhere. Exoplanet cloud particles are made of a mix of materials (V_s/V_{tot} , $s=\text{TiO}_2$, Fe, MgSiO₃ etc, top right) which changes with atmospheric temperature (black line in top left), hence location. The dust-to-gas ratio (ρ_d/ρ_{gas}) demonstrates where the main cloud mass is located. It is correlated to the cloud column density ($\rho_{\text{coll}}^{\text{cloud}}$; both bottom left). The mean cloud particle sizes ($\langle a \rangle$ [μm]) are different at different atmospheric heights (dashed blue line in bottom right) ranging from 10^{-6}cm at the top of the cloud to $>0.5\mu\text{m}$ at the cloud bottom. Local particle sizes deviate from this mean value (σ_a – standard deviation; red and green lines) most in the area of strongest surface growth $\sim 10^{-6}$ bar. The largest particles reside in the densest part of the atmosphere and are made of high-temperature condensates like CaTiO₃[s] and Al₂O₃[s].

- the seed formation rate, J^* [s⁻¹] (top left panel),
- the material volume fractions, V_s/V_{tot} (V_s – local volume fraction of the material s , V_{tot} – total, local cloud volume, s – solid material like TiO₂[s], SiO[s] etc.; top right panel),
- the cloud and gas column densities, ρ_{coll} [g cm⁻²], the cloud mass load of the atmosphere in terms of the ratio between cloud mass density and gas mass density, ρ_d/ρ_g , and the cloud

column density, $\rho_{\text{coll}}^{\text{cloud}}$ (bottom left),

– and the mean cloud particle radii, $\langle a \rangle$ [μm] (bottom right).

The cloud column density (ρ_{col} [g cm^{-2}]) is the integrated local cloud particle number density (number of cloud particles per volume) over the geometrical extension of the cloud. The number of particles that make up the whole cloud is determined by the seed formation rate (J_* [s^{-1}]). Both, TiO_2 and SiO form condensation seeds. Carbon does not form as we consider a gas that has more oxygen than carbon ($\text{C/O}=0.53$). SiO seed formation is most efficient at lower temperature/pressures and TiO_2 picks up at higher temperatures. The whole region of efficient seed formation ($J_* > 10^{-8} \text{ s}^{-1}$) spans about 4 orders of magnitude in pressure in the upper atmospheric regions with $p < 10^{-4} \text{ bar}$. (Note that the same panel shows the atmospheric (T, p) structure in black on the right axis for comparison.). The emergence of the condensation seeds is also apparent from the panel showing the material composition of the cloud particles (top right): The uppermost, low pressure regions are made solely of very small $\text{TiO}_2[\text{s}]$ and $\text{SiO}[\text{s}]$ condensation seeds (*haze*). The bulk of the cloud particle volume forms through condensation (surface reactions) of all materials at $p > 10^{-8} \text{ bar}$. At the cloud centre ($p \approx 10^{-6} \text{ bar}$) cloud particles are made of a mix of $\text{Mg}_2\text{SiO}_4[\text{s}]$ (20%), $\text{Fe}_2\text{SiO}_4[\text{s}]$ (17.5%) and $\text{MgSiO}_3[\text{s}]$ (16.5%), and $\text{MgO}[\text{s}]$, $\text{SiO}_2[\text{s}]$ and $\text{SiO}[\text{s}]$ form circa 15% each of the total cloud material. All other materials occur as inclusions with $\lesssim 10\%$. Silicate materials evaporate at $p \approx 10^{-3} \text{ bar}$ (here: $T \approx 1700\text{K}$). The innermost cloud layers are made of high-temperature condensates (materials that are thermally stable at high temperatures) like $\text{Fe}[\text{s}]$, $\text{CaTiO}_3[\text{s}]$ and $\text{Al}_2\text{O}_3[\text{s}]$. The consistent solution of the cloud formation processes allows us now to link the cloud material composition with the resulting cloud particle sizes (lower right). We start our discussion again in the low pressure upper atmosphere region which is dominated by the nucleation process. Here we find that the cloud particles remain very small ($\approx 10^{-3} \mu\text{m}$) until exactly where the bulk growth sets in efficiently. The mean particles size, $\langle a \rangle$ (dashed blue line), increases steadily inwards because gravitational settling causes the cloud particles to fall into atmospheric regions of higher densities but also of increasing temperature. Note that the cloud expands beneath the nucleation zone. The high densities accelerate the surface growth processes leading to the steep inward increase of the cloud particle's mean radius (and their fall speed; not shown) until they encounter the temperatures that cause complete evaporation. The inwards increasing particle sizes do cause an increase of the atmosphere's cloud mass load (lower left, brown dashed line): The ratio between the cloud mass density and the gas density, ρ_d/ρ_g (so-called 'dust-to-gas ratio'), is largest where the mean particle sizes reach their maximum.

Cloud particles develop not only a vertical size distribution $f(a(z))$ (blue dashed line, lower right panel Fig. 3), but appear with a local size distribution $f(a(z), z)$. This can, for example, be represented by a Gaussian distribution with a standard deviation, $\sigma_a(z)$ (solid green and red line in lower right panel)¹⁴. The local size distributions are very narrow in the low-density cloud regions ($p < 10^{-9} \text{ bar}$ for the model shown) and at the cloud base ($p > 10^{-4} \text{ bar}$ for the model shown). The size distribution broadens when the bulk

¹⁴For this paper, the height dependent parameters, $N(z, a)$ and $\sigma(z)$, for a Gaussian distribution, $f(a, N) = N/(2\pi^2\sigma) \cdot \exp(-[(a - \langle a \rangle)/\sigma]^2)$, are derived using dust moments $L_j(z) = \int_{V_1}^{\infty} V(z)^{j/3} f(V, z) dV$ as described in Helling et al. (2008b). $N(z, a)$ is the number of cloud particles at a certain height $z=z(p, T)$ of a certain size a , and $\sigma(z)$ is the local standard deviation, $V(z)$ is the local cloud particle volume.

growth sets in. The width of the size distribution is also determined by the nucleation process. It is the widest when the second nucleation peak appears due to the inset of efficient TiO_2 nucleation ($p \approx 10^{-6}$ bar for the model shown). At this location, the size distribution contains a considerable number of smaller cloud particles. In conclusion, in order to present the local cloud particle size distribution, all size determining processes need to be consistently treated. Powell et al. (2018) do present results for double-peaked local particle size distribution based on a binning method.

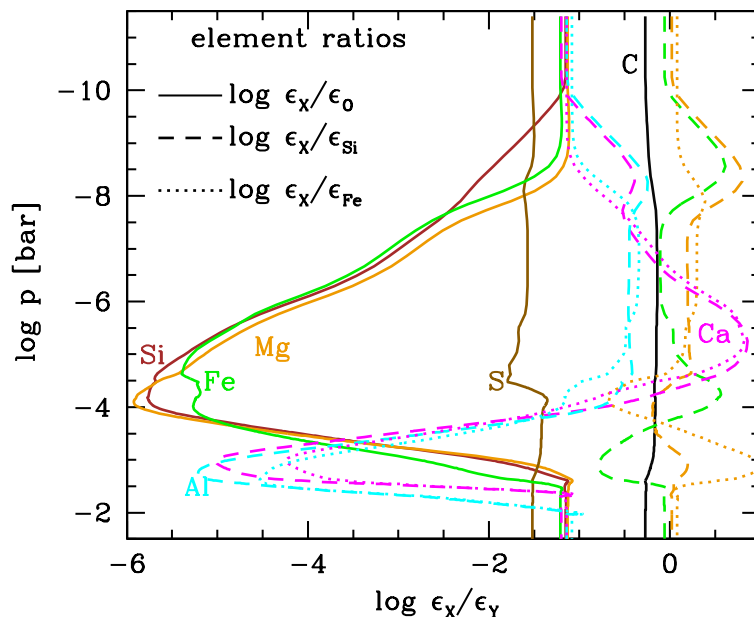


Figure 4

Element abundance ratios (mineralogic ratios) in relation to oxygen (O, solid lines), silicon (Si, dashed lines) and iron (Fe, dotted lines) on a logarithmic scale for the same model like in Fig. 3. The individual elements are colour coded. The C/O ratio is indicative of an oxygen rich gas with the unperturbed, solar value of $C/O=0.537$ above and below the cloud. The maximum value reached in this giant gas planet atmosphere model is $C/O=0.725$.

4.1. Thoughts on model completeness

The question arises in how far the above drawn picture of clouds on exoplanets is complete. It is incomplete in the sense that not all possible thermally stable materials have been included and that only those resulting from the most abundant (solar) elements were considered. The alternative to this is to apply a phase equilibrium (thermal equilibrium; see Marley & Robinson 2015) approach which, however, will not provide information about, for example, particle sizes nor knowledge about if these materials would actually form for a given atmospheric condition. We have derived the principle characteristics for exoplanet clouds based on a 1D atmosphere configuration. This naturally neglects all multi-dimensional effects like equatorial jets, turbulence, or scattering of stellar photons beyond the day-night terminator, but it is the only way to build our understanding based on a consistent theoretical approach. This knowledge can then be applied to 3D radiation-

hydrodynamics models including all the required gas and cloud chemistry (Lee et al. 2016; Lines et al. 2018), or inform retrieval models. Retrieval models necessarily use a 1D atmospheric profile that require heavy parameterisation to allow the simulation of grids of 10^6 atmosphere structures. However, as it turns out, the parameterised temperature profiles resemble 3D structures well if enough parameters are allowed and if high resolution and more data points are included (Blecic et al. 2017). Furthermore, exoplanet atmospheres are exposed to external radiation from the host star but also from high-energy cosmic rays leading to atmospheric electrification (Helling et al. 2016a). The host-star’s UV field ionises the upper atmospheric regions for close-in planets and so does the interplanetary radiation field for the more distant planets in a planetary system. Cosmic ray particles arrive with a far higher energy, though on a lower rate, and reach deeper atmospheric layers or even the planetary surface where they trigger the appearance of HCN (Airapetian et al. 2016). In addition, photon-initiated chemistry (oppose to chemical reactions occurring due to the collision between two gas species) occurs in the outermost layers of an exoplanet atmosphere. The formation of photochemical haze in form of large carbo-hydrate molecules is discussed to require a combination of gas-phase photochemistry and coagulation (collisional reaction between exiting particles) of photochemical educts which then produce so-called tholins (Kawashima & Ikoma 2018). Tholins (Sagan & Khare 1979), describe a variety of organic compounds that are not specified any further.

4.2. Summary of take-away points about clouds in exoplanet atmospheres

1. Small, haze-sized aerosols constitute the upper boundary of clouds.
2. The seed formation rate determines the number of cloud particles.
3. Any middle part of a cloud will be chemically very rich. Cloud particles are made of a mix of all thermally stable materials. An optically thick atmosphere results.
4. Cloud particle radii and their material composition change throughout the cloud because of changing thermodynamic conditions.
5. Large cloud particles made of high-temperature condensates form the cloud base.

5. Exoplanet element abundances and mineralogic ratios

The original element abundances (i.e. the number of elements of one kind contained in all gas species which has not yet been affected by cloud formation) that determine the chemical composition of an exoplanet’s atmosphere gas may reflect its formation processes (e.g. Helling et al. 2014; Carter et al. 2015; Cridland et al. 2016; Eistrup et al. 2016; Madhusudhan et al. 2017). Hence, attempts are ongoing to use element abundance measurements from exoplanet atmospheres to constrain planet formation processes (e.g. Pinhas et al. 2016). It will, however, be challenging to determine the values of the initial element abundances from spectroscopy of the exoplanet atmosphere if clouds have formed. Cloud nucleation and growth consume elements, therefore causing specific atoms and molecules to drop in abundance. Transport processes like gravitational settling or advection will de-localise the process. Linking the observed atmospheric exoplanet element abundances to the host star’s element abundances is therefore a non-trivial task, unless a complex (i.e. as complete as possible) modelling approach is adopted. It appears more feasible to address the relation between the host star’s element abundances and the element abundance of the planet’s core (e.g. Santos et al. 2017). The challenges hereby, however, lay with the precise measurement

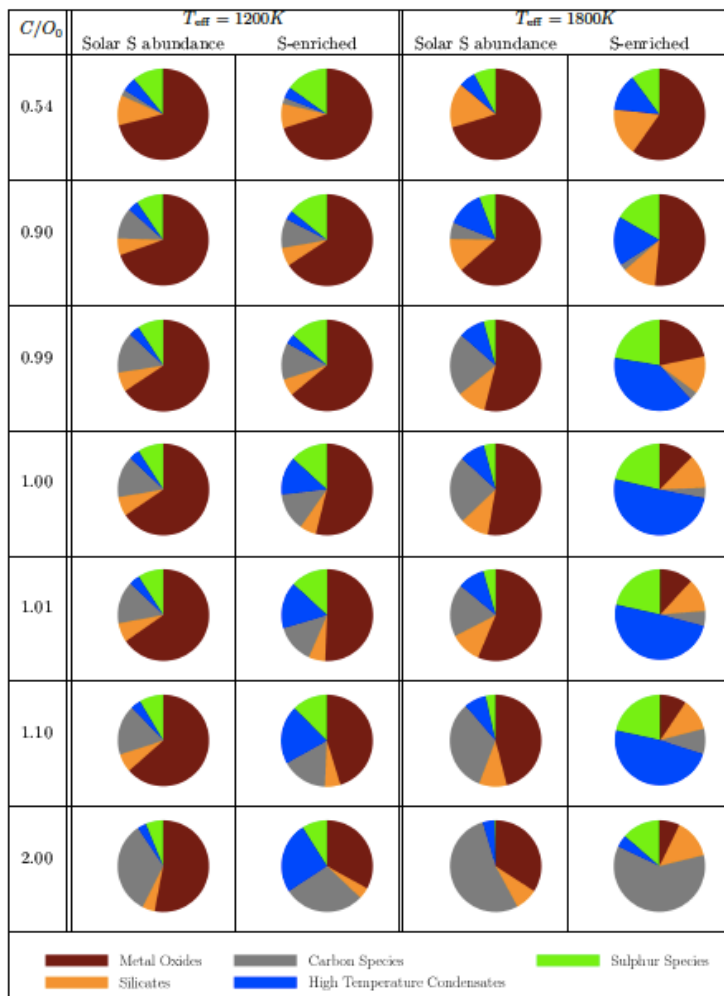


Figure 5

The cumulative cloud material volume fractions for a set of 1D DRIFTPHOENIX model atmospheres for varying carbon-to-oxygen ratio (C/O) and sulphur abundance. The focus of this figure is the transition from an oxygen-rich to a potentially carbon-rich atmosphere: Carbon condensation occurs already at $C/O=0.9$ (and lower for lower T_{eff}) but is suppressed upto $C/O \approx 1.1$ by an increase of sulphur in particular in warmer atmospheres. The cloud material species were combined in 5 groups: metal oxides ($\text{SiO}[\text{s}]$, $\text{SiO}_2[\text{s}]$, $\text{MgO}[\text{s}]$, $\text{FeO}[\text{s}]$), silicates ($\text{MgSiO}_3[\text{s}]$, $\text{Mg}_2\text{SiO}_4[\text{s}]$), carbon species ($\text{C}[\text{s}]$, $\text{SiC}[\text{s}]$, $\text{TiC}[\text{s}]$), high temperature condensates ($\text{TiO}_2[\text{s}]$, $\text{Al}_2\text{O}_3[\text{s}]$, $\text{CaTiO}_3[\text{s}]$, $\text{Fe}[\text{s}]$), and sulfur species ($\text{S}[\text{s}]$, $\text{MgS}[\text{s}]$, $\text{FeS}[\text{s}]$).

of the stellar properties as demonstrated for example for 55 Cnc e (Crida et al. 2018). Matters are further complicated if the element abundances are derived from observations of molecules that are (additionally) affected by photochemistry (e.g. CO/CH_4 , N_2/NH_3) in the atmospheric gas above the cloud layer (e.g. Moses et al. 2016) or cosmic ray impact (Rimmer et al. 2014). Figure 4 summarises the element depletion by cloud formation in

terms of element ratios (also called mineralogic ratios), $\log \epsilon_X/\epsilon_O$ (solid lines), $\log \epsilon_X/\epsilon_{Si}$ (dashed lines), and $\log \epsilon_X/\epsilon_{Fe}$ (dotted lines) for the same exoplanet atmosphere as in Fig. 3. The most interesting is the carbon-to-oxygen ration (C/O) which varies between the initial solar value of ≈ 0.54 and ≈ 0.73 . This emphasises that there is no one C/O that can be used to characterise a cloud-forming exoplanet. Such a change of C/O due to cloud formation can convert the gas-phase chemistry from an oxygen-dominated into a carbon-dominated gas if C/O is already ≥ 0.85 as result of planet formation processes (Helling et al. 2014; Madhusudhan et al. 2017). Molecules like e.g. C_2H_2 , HCN, CH and polycyclic-aromatic-hydrocarbon (PAH) molecules can then be expected to appear in the exoplanet absorption spectrum (Bilger et al. 2013) where photochemistry is inefficient. The ratios Fe/O, Si/O and Mg/O are rather similar as the depleting materials are thermally stable at similar temperatures, and Fe/Si/Mg have comparable initial element abundances. Sulphur appears to play no substantial role for element depletion in warm giant gas planets. The Mg/Si maximum is ≈ 1.56 , the minimum is ≈ 0.64 compared to a solar value of 1.05. The Fe/Si maximum is ≈ 3.66 , its minimum ≈ 0.16 compared to a solar value of 0.87. We note that the precise local values of the mineralogic values will depend on whether the element replenishment is convective or diffusive. The maximum/minimum values cited here should, however, be independent of the element replenishment mechanism.

In Figure 5, the effect of C/O on the cloud material distribution is reviewed for distant giant gas planets of two different effective temperatures (cold vs warm). For simplification, 1D cumulative global values were adopted for five groups of materials: metal oxides (SiO[s], SiO₂[s], MgO[s], FeO[s]), silicates (MgSiO₃[s], Mg₂SiO₄[s]), carbon species (C[s], SiC[s], TiC[s]), high temperature condensates (TiO₂[s], Al₂O₃[s], CaTiO₃[s], Fe[s]), and sulfur species (S[s], MgS[s], FeS[s]). KCl[s] and S[s] appeared to be negligible (as nucleation species and as growth species), hence, it will have little impact on the gas chemistry. In the solar system case (left columns), metal oxides and silicates are the volume dominating condensates except in the case of a carbon-rich, warm exoplanet. Carbon-binding materials never dominate the cloud particle material in the summarised cases where C/O changes from oxygen-rich (C/O=0.54) to carbon-rich (C/O=1.1), except for the warm model for C/O=2.0. Sulfur haze has been suggested to emerge in cold gas giants (<700K, Gao et al. 2017). An overabundance of sulfur was confirmed for Uranus (H₂S ice particles detected, see de Pater 2018), and volcanic sulfur as trigger for snowball Earth (Macdonald & Wordsworth 2017). Figure 5 contains a first summary in how far an increased sulfur abundance affects the cloud composition in combination with a varying C/O. The sulfuric species included in this test do not contribute much to the cloud material volume in the solar sulfur abundance cases. Sulfur plays a larger role as part of condensates in the warmer atmosphere in the chemical transition region of C/O=0.99...1.1.

5.1. Summary of take-away points on element abundances in exoplanet atmospheres

1. Spectroscopically observed element abundances of exoplanets are altered by cloud formation and photochemistry.
2. No one carbon-to-oxygen ratio characterises an exoplanet atmosphere.
3. No one mineralogical ratio characterises an exoplanet atmosphere.
4. Observed carbon-rich exoplanets maybe camouflaged cloud-forming oxygen-rich exoplanets.

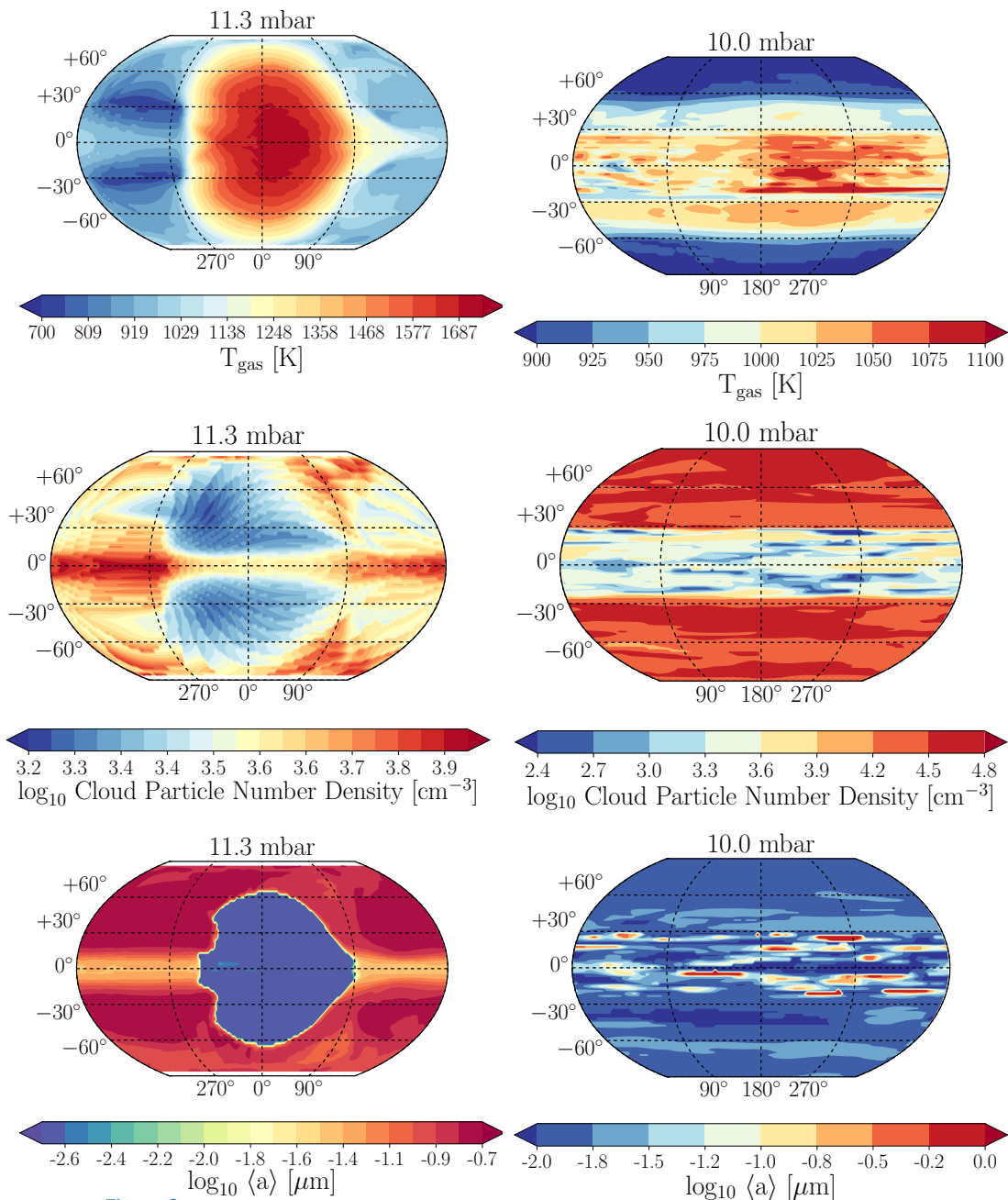


Figure 6

Maps of 3D GCM models with cloud formation for HD189733b (left; Lee et al. 2016) and for HD 209458b (right; Lines et al. 2018). **Top:** gas temperature map, **Centre:** cloud particle number density, **Bottom:** mean cloud particle radii. Both hot Jupiter atmospheres were modelled with different codes such that their latitude grid is offset by 180° to each other. The point of strongest heating (the substellar point) is for both planets at the equator but at the latitude of 0° for HD 189733b (left) and at the latitude of 180° for HD 209458b (right).

6. Cloudy weathers on extrasolar planets

Forecasting weather on Earth had reached a new level of reliability when high-performance computations were applied to solve the 3D radiation hydrodynamics, i.e. the equations that forecast the motion of the atmospheric gas including heating and cooling in 3D. Such models are called global circulation models (GCMs). The modelling results were compared to and combined with superb observational data on, for example, precipitation with respect to particle sizes and their numbers at different locations. Nevertheless, the Intergovernmental Panel on Climate Change (IPCC¹⁵) has identified the effect of aerosols and precursors as carrying the largest uncertainty among the drivers for climate change on Earth. No such constraints are available for exoplanets yet. Seen from Earth, evidence for weather-like variability on extrasolar planets is provided by phase curves that show hot spots leading or trailing the point of highest stellar flux input (substellar point). Nine out of 11 planets show a $4.5\mu\text{m}$ -phase-curve consistent with an east-ward hotspot off-set (giant-gas planets: HD189744b – Knutson et al. (2007), HD209458b – Zellem et al. (2014), WASP-12b – Cowan et al. (2012), WASP-14b – Wong et al. (2015), WASP19b & HAT-P-7b – Wong et al. (2016), WASP-18b – Maxted et al. (2013), WASP-43b – Angelo & Hu (2017); super-Earth: 55 Cnc e – Keating & Cowan (2017)). The hot Jupiter Kepler-7b¹⁶ was the first planet detected which had its hottest atmospheric spot off-set to the West (instead to the East; compare Fig. 6). This observation is attributed to high-altitude, optically reflective clouds located west-ward off the substellar point (Demory et al. 2013). CoRoT-2b¹⁷ is the first hot Jupiter with a west-ward offset of the hot-spot that is suggested to be caused by a westward wind due to non-synchronous rotations, magnetic effects, or maybe partial cloud coverage (Dang et al. 2018). The partial cloud coverage is supported by a featureless dayside emission spectrum of CoRoT-2b. Applying 3D cloud-free radiation-hydrodynamics simulation equatorial jets were established to be the leading cause of such hot-spots, but additional mechanisms like clouds were required to explain the observed light curves (Komacek et al. 2017).

Global circulation models are extremely time consuming, even more so if sophisticated descriptions of microphysical processes like cloud formation and radiation transfer are included. Systematic studies of dynamic features of giant gas planets were therefore conducted based on cloud- and chemistry-free 3D GCMs (e.g. Kataria et al. 2016) or with cloud particles as passive opacity source (e.g. Parmentier et al. 2018). Carone et al. (2018) summaries how the tropospheric circulation states change depending on planetary radius and orbital distance for tidally locked terrestrial planets: Close-in orbits of 1 day drive equatorial superrotation and high-latitude jets (e.g. on TRAPPIST-1b¹⁸). The equatorial superrotation prevails for increasing orbit of ~ 10 days (e.g. TRAPPIST-1g). Radial flows drive the atmospheric motion for orbital periods less than 20 days (e.g. GJ667Cf) as the external heating through irradiation has decreased drastically. Similar flow pattern will appear in hot Jupiters where the equatorial superrotation prevails for cloud-free 3D GCM's for

¹⁵<http://www.ipcc.ch/>

¹⁶Kepler is a space telescope built to discover extrasolar planets: https://www.nasa.gov/mission_pages/kepler.

¹⁷CoRoT stands for Convection, Rotation and planetary Transits: <https://corot.cnes.fr/en/COROT/index.htm>.

¹⁸TRAPPIST stands for Transiting Planets and Planetesimals Small Telescope which is operated at the La Silla Observatory in Chile: <https://en.wikipedia.org/wiki/TRAPPIST>.

HAT-P1b¹⁹, HAT-P-12b, WASP-6b²⁰, WAS-17b, WASP-19b, WASP-31b, WASP-39b, but also for HD 189733b and HD 209458b (Kataria et al. 2016). It, however, remains to be seen in how far different numerical approaches of treating the full 3D radiation hydrodynamics (Dobbs-Dixon & Agol 2013; Mayne et al. 2014; Mendonça et al. 2016) and variations of 2D+1 hydrodynamics (1 dimension treated in hydrostatic equilibrium; Parmentier et al. 2013; Komacek et al. 2017; Carone et al. 2018) and additional processes (cloud formation, magnetic coupling) influence the emergence of superrotation (i.e. extremely fast moving atmospheric gas).

The time-consumption increases substantially if cloud formation and gas-phase chemistry are included as consistent part of the 3D radiation-hydrodynamics simulations for exoplanets. Only two planets have therefore been models so far (HD 189733b – Lee et al. 2016 and HD 209458b – Lines et al. 2018), and no long-term studies were conducted so far. It was shown that cloud particles of different sizes and compositions are distributed throughout the whole computational domain of the modelled atmosphere. Hence, both planets’ atmospheres are affected by cloud formation. Figure 6 (left: HD 189733b, right: HD 209458b) shows the 3D maps for the gas temperature (T_{gas} [K]), the number density of cloud particles (n_d [cm^{-3}]) and mean cloud particle radii ($\langle a \rangle$ [μm]) at the pressure level of $\approx 10^{-2}$ bar. Both planets show an off-set of the hottest part of the atmosphere to the East and the temperature maps demonstrate that the hydrodynamic transport (wind) is faster than the radiative cooling of the atmospheric gas. This has strong implications for the cloud distribution which is most obvious for HD 189733b at this pressure level. The cloud particle size map correlated well with the temperature map in that the particles are the smallest where the atmospheric gas is the hottest. Consequently, the cloud particle size maps the eastward off set of the temperature. The northern and southern hemispheres on HD 189733b contain larger cloud particles than the equatorial jet-stream region. For HD 209458b, the equatorial region shows spots with large cloud particles whereas the northern and southern hemisphere are populated with small cloud particles. This is a result of more cloud particles being present in the equatorial region in HD 189733b and less in the hemispheres, and less cloud particles being present in the equatorial region in HD 209458b and more in the hemispheres at this pressure level. Figure 6 further shows how different the two giant-gas planets are regarding their weather appearance. HD 209458b forms three distinct cloud bands, the retrograde moving northern and southern hemisphere and the prograde moving equatorial belt. The wave-flow pattern in the equatorial belt does imprint on the cloud particle sizes appearing as patchy distribution in Fig. 6 also in these low-pressure regions. HD 189733b has a distinct cloud distribution in the hot-spot area, in the northern and southern hemispheres and in the equatorial region. This pattern prevails higher up in the atmosphere where the gas pressure is lowest.

Both planets, HD 189733b and HD 209458b, were classified as hot Jupiters but small differences like in planetary mass and planetary radius ($M_{\text{HD189b}} \sim 1.3M_J$, $M_{\text{HD209b}} \sim 0.69M_J$; $R_{\text{HD189b}} \sim 1.138R_J$, $M_{\text{HD209b}} \sim 1.38R_J$) affect the pressure stratification of the atmosphere. The amount of external energy input is different due to differences in the semi-major axis ($a_{\text{HD189b}} \sim 0.031\text{AU}$, $a_{\text{HD209b}} \sim 0.047\text{AU}$; i.e. the distance to the host star). Both effects combined cause substantial differences in the local gas densities and gas temperatures which strongly influence the local gas chemistry, and hence, the local cloud

¹⁹HAT stands for Hungarian-made Automated Telescope Network: <https://hatnet.org>.

²⁰WASP stands for Wide Angle Search for Planets: <https://wasp-planets.net>.

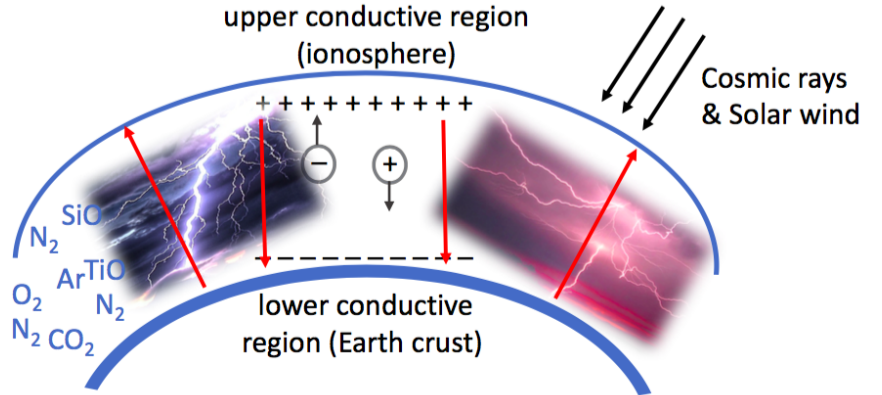


Figure 7

The global electric circuit (red arrows) forming in exoplanet atmospheres due to lightning activities in exoplanet clouds, the formation of an ionosphere through external irradiation (Cosmic rays, solar wind) and a inner, conductive boundary.

formation processes. A discussion comparing the cloud properties of both planets in 1D is provided in (Helling et al. 2016b).

6.1. Lightning on exoplanet and the extrasolar global electric circuit

The CLOUD experiment at CERN²¹ demonstrated (though only for a very limited temperature range) that cloud formation expands into higher atmospheric regions on Earth due to cosmic rays open chemical channels to form condensation seeds from ionised gas species. The process becomes inefficient with increasing density, hence deeper inside the atmosphere. Similar effect would occur for exoplanets where cosmic rays, stellar and interstellar radiation affects the gas ionisation in the upper atmosphere such that an ionosphere may form (e.g. Rimmer & Helling 2013; Rimmer et al. 2014; Rodriguez-Barrera et al. 2018). The ionisation of the gas above the cloud cause a current which ionises the upper cloud layers like on Earth, and the atmosphere will become electrified. Inside the cloud, turbulence-driven collisional processes cause triboelectric charging (see Sect. 2.1 in Helling et al. 2016a) as the atmosphere is very dynamic also on small scales (Helling et al. 2004, 2011). Gravitational settling establishes a vertical, large-scale charge separation (see Fig. 7). The advection of aerosols that closely follow the gas motion due to frictionally coupling may cause similar effects in horizontal directions. In consequence, an electrostatic potential difference builds up in various parts of the atmosphere. This potential can discharge in form of leaking currents or in form of intra-cloud lightning. Leaking currents (‘fair-weather current’) will only occur in cloud-free (parts of) atmospheres, and lightning only in cloudy (parts of) atmospheres. Lightning has been detected on many of the cloudy solar system planets at optical and radio wavelengths, but a good statistical sampling of the lightning occurrence rate is only available for Earth (Hodosán et al. 2016a). Lightning occurrence rates differ for oceans and continents on Earth, and hence, may provide a probe for different exoplanet

²¹<https://home.cern/about/experiments/cloud>

environments.

On Earth, lightning plays a major role for feeding what is called a 'global electric circuit' by its return current. The Global Electric Circuit is a current system that affects the Earth weather systematically on large and on global scales. The criteria for an extrasolar global electric circuit include not only global charge-separation processes and current flows, but also globally prevalent upper and lower conductive regions (Sect. 3.3 in Helling et al. 2016a; see Fig. 7). The upper conductivity region is the ionosphere, and the lower conductivity region will be a rocky planet's crust or the thermally ionised inner, hot part of a giant gas planet's atmosphere. It will remain to be seen which role a global electric circuit has in extrasolar planets which so far have been observed to possess very dynamical atmospheres with clouds. Maybe electric circuits will therefore occur on more local, smaller scales in giant exoplanets compared to smaller, Earth-like planets with less dramatic hydrodynamics.

In addition to lightning being one of the key elements of a global electric circuit, lightning dramatically affects the local chemistry by converting a cold gas into a plasma, hence, by changing its thermodynamic state from a cold ($\sim 1000\text{K}$) into a very hot gas ($\sim 30,000\text{K}$). Possible extrasolar lightning tracer are chemical species like HCN and C_2H (Rimmer & Helling 2016; Hodosán et al. 2016b; Ardaseva et al. 2017), or spectral peculiarities like lightning modulated coherent cyclotron emission coming from electrons that are accelerated by the planet's magnetic field (Vorgul & Helling 2016; Helling & Vorgul 2017) similar to the lightning modulated cosmic ray air showers recently discovered on Earth (Schellart et al. 2015; Trinh et al. 2017). Moreover, strong large-scale magnetic fields like on Saturn (or Brown Dwarfs) enhance lightning-induced electric fields producing strong transient optical emission as demonstrated for Earth (Pérez-Invernón et al. 2017). As lightning requires the presence of clouds, lightning indicators are formidable tool to prove the presence of clouds in exoplanet atmosphere as well as gaining insight into the atmospheric dynamics. If electric circuit systems form on global scales, it will provide a mechanisms to link atmospheric processes globally.

6.2. Summary of take-away points in 3D extrasolar clouds

1. Horizontal advection of gas and cloud particles leads to zonal pattern like bending and hot-spots on exoplanets, similar to Jupiter.
2. Temporary effects on cloud particle distribution cause a time-variable opacity leading to time-dependent thermal emissions and spectral features.
3. Exoplanet clouds can cause lightning which affects the local gas chemistry.
4. Exoplanet atmospheres may establish a global electric circuit that can link atmospheric process over large distances non-locally.

7. Future issues

With many satellites and instruments becoming available to analyse exoplanet atmospheres, cloud formation has turned into a growing research area that combines the need for extending laboratory work (e.g. Rietmeijer et al. 1999; Gadallah et al. 2013; Sabri et al. 2014; He et al. 2018) to more extreme conditions with that for a fundamental understanding of phase-transition/cluster chemistry (e.g. Jeong et al. 2000; Patzer et al. 2002; Lee et al. 2015; Decin et al. 2017; Gobrecht et al. 2017), the exchange with solar system research (Helling et al. 2016a) and complex modelling. While first fully consistent atmosphere models for

extrasolar planets have emerged in 1D and in 3D, approximations are still applied in 1D retrieval methods and in most 3D simulations in order to limit the demand on computing times. Such approximations do impact the accuracy of the local temperature which in turn affects the local chemistry which determines the spectral appearance. Similar arguments hold for the treatment of the radiative transfer problem, but here the stellar literature holds a reservoir (e.g. Gustafsson 2008; Hubeny 2017) to build on well established experiences in 1D and in 3D set-ups of varying, wavelength-dependent optical depths.

Future observations will most likely continue to demonstrate the large diversity of extrasolar planets of which none resembles any solar system planet exactly. Venus, Earth and Mars demonstrate how seemingly small differences cause planets to evolve into very different states. The most pressing future issue is therefore to enable complex, theoretical modelling in tandem with elaborate machine learning tools in order to combine the limited number of observations per exoplanet such that we are able to make predictions about the missing information like time-evolution, long-term behaviour (climate) and maybe even habitability on cosmological scales.

DISCLOSURE STATEMENT

If the authors have nothing to disclose, the following statement will be used: The authors are not aware of any affiliations, memberships, funding, or financial holdings that might be perceived as affecting the objectivity of this review.

ACKNOWLEDGMENTS

David Gobrecht is thanked for providing the $(\text{Al}_2\text{O}_3)_N$ cluster structures. Jasmina Blecic, Ian Boutle, and Ludmila Carone are thanks for valuable discussions on the manuscript. Stefan Lines and Graham Lee are thanked for providing maps of 3D GCM results.

LITERATURE CITED

- Airapetian VS, Glocer A, Gronoff G, Hébrard E, Danchi W. 2016. Prebiotic chemistry and atmospheric warming of early Earth by an active young Sun. *Nature Geoscience* 9:452–455
- Angelo I, Hu R. 2017. A Case for an Atmosphere on Super-Earth 55 Cancri e. *AJ* 154:232
- Apai D, Karalidi T, Marley MS, Yang H, Flateau D, et al. 2017. Zones, spots, and planetary-scale waves beating in brown dwarf atmospheres. *Science* 357:683–687
- Apai D, Radigan J, Buenzli E, Burrows A, Reid IN, Jayawardhana R. 2013. HST Spectral Mapping of L/T Transition Brown Dwarfs Reveals Cloud Thickness Variations. *ApJ* 768:121
- Arcangeli J, Désert JM, Line MR, Bean JL, Parmentier V, et al. 2018. $\text{H}^?$ Opacity and Water Dissociation in the Dayside Atmosphere of the Very Hot Gas Giant WASP-18b. *ApJL* 855:L30
- Ardaseva A, Rimmer PB, Waldmann I, Rocchetto M, Yurchenko SN, et al. 2017. Lightning chemistry on Earth-like exoplanets. *MNRAS* 470:187–196
- Bilger C, Rimmer P, Helling C. 2013. Small hydrocarbon molecules in cloud-forming brown dwarf and giant gas planet atmospheres. *MNRAS* 435:1888–1903
- Blecic J, Dobbs-Dixon I, Greene T. 2017. The Implications of 3D Thermal Structure on 1D Atmospheric Retrieval. *ApJ* 848:127
- Carone L, Keppens R, Decin L, Henning T. 2018. Stratosphere circulation on tidally locked ExoEarths. *MNRAS* 473:4672–4685
- Carter PJ, Leinhardt ZM, Elliott T, Walter MJ, Stewart ST. 2015. Compositional Evolution during Rocky Protoplanet Accretion. *ApJ* 813:72

- Charnay B, Bézard B, Baudino JL, Bonnefoy M, Boccaletti A, Galicher R. 2018. A Self-consistent Cloud Model for Brown Dwarfs and Young Giant Exoplanets: Comparison with Photometric and Spectroscopic Observations. *ApJ* 854:172
- Cowan NB, Machalek P, Croll B, Shekhtman LM, Burrows A, et al. 2012. Thermal Phase Variations of WASP-12b: Defying Predictions. *ApJ* 747:82
- Crida A, Ligi R, Dorn C, Lebreton Y. 2018. Mass, radius, and composition of the transiting planet 55 Cnc e : using interferometry and correlations. *ArXiv e-prints*
- Cridland AJ, Pudritz RE, Alessi M. 2016. Composition of early planetary atmospheres - I. Connecting disc astrochemistry to the formation of planetary atmospheres. *MNRAS* 461:3274–3295
- Dang L, Cowan NB, Schwartz JC, Rauscher E, Zhang M, et al. 2018. Detection of a westward hotspot offset in the atmosphere of hot gas giant CoRoT-2b. *Nature Astronomy* 2:220–227
- de Pater I. 2018. Selective enrichment of volatiles confirmed. *Nature Astronomy* 2:364–365
- Decin L, Richards AMS, Waters LBFM, Danilovich T, Gobrecht D, et al. 2017. Study of the aluminium content in AGB winds using ALMA. Indications for the presence of gas-phase $(\text{Al}_2\text{O}_3)_n$ clusters. *A&A* 608:A55
- Demory BO, de Wit J, Lewis N, Fortney J, Zsom A, et al. 2013. Inference of Inhomogeneous Clouds in an Exoplanet Atmosphere. *ApJL* 776:L25
- Diamond-Lowe H, Berta-Thompson Z, Charbonneau D, Kempton EMR. 2018. Ground-based optical transmission spectroscopy of the small, rocky exoplanet GJ 1132b. *ArXiv e-prints*
- Dobbs-Dixon I, Agol E. 2013. Three-dimensional radiative-hydrodynamical simulations of the highly irradiated short-period exoplanet HD 189733b. *MNRAS* 435:3159–3168
- Dunne EM, Gordon H, Kürten A, Almeida J, Duplissy J, et al. 2016. Global atmospheric particle formation from CERN CLOUD measurements. *Science* 354:1119–1124
- Eistrup C, Walsh C, van Dishoeck EF. 2016. Setting the volatile composition of (exo)planet-building material. Does chemical evolution in disk midplanes matter? *A&A* 595:A83
- Gadallah KAK, Mutschke H, Jäger C. 2013. Analogs of solid nanoparticles as precursors of aromatic hydrocarbons. *A&A* 554:A12
- Gao P, Marley MS, Zahnle K, Robinson TD, Lewis NK. 2017. Sulfur Hazes in Giant Exoplanet Atmospheres: Impacts on Reflected Light Spectra. *AJ* 153:139
- Glawe C, Schmidt H, Kerstein AR, Klein R. 2015. XLES Part I: Introduction to Extended Large Eddy Simulation. *ArXiv e-prints*
- Gobrecht D, Cristallo S, Piersanti L, Bromley ST. 2017. Nucleation of Small Silicon Carbide Dust Clusters in AGB Stars. *ApJ* 840:117
- Goeres A. 1996. Chemistry and thermodynamics of the nucleation in R CrB star shells, In *Hydrogen Deficient Stars*, eds. CS Jeffery, U Heber, vol. 96 of *Astronomical Society of the Pacific Conference Series*
- Gustafsson B. 2008. An attempt to summarize and conclude. *Physica Scripta Volume T* 133:014041
- Gustafsson B, Edvardsson B, Eriksson K, Jørgensen UG, Nordlund Å, Plez B. 2008. A grid of MARCS model atmospheres for late-type stars. I. Methods and general properties. *A&A* 486:951–970
- He C, Horst SM, Lewis NK, Yu X, Moses JJ, et al. 2018. Photochemical Haze Formation in the Atmospheres of super-Earths and mini-Neptunes. *ArXiv e-prints*
- Helling C, Ackerman A, Allard F, Dehn M, Hauschildt P, et al. 2008a. A comparison of chemistry and dust cloud formation in ultracool dwarf model atmospheres. *MNRAS* 391:1854–1873
- Helling C, Fomins A. 2013. Modelling the formation of atmospheric dust in brown dwarfs and planetary atmospheres. *Philosophical Transactions of the Royal Society of London Series A* 371:20110581–20110581
- Helling C, Harrison RG, Honary F, Diver DA, Aplin K, et al. 2016a. Atmospheric Electrification in Dusty, Reactive Gases in the Solar System and Beyond. *Surveys in Geophysics* 37:705–756
- Helling C, Jardine M, Mokler F. 2011. Ionization in Atmospheres of Brown Dwarfs and Extrasolar Planets. II. Dust-induced Collisional Ionization. *ApJ* 737:38

- Helling C, Klein R, Woitke P, Nowak U, Sedlmayr E. 2004. Dust in brown dwarfs. IV. Dust formation and driven turbulence on mesoscopic scales. *A&A* 423:657–675
- Helling C, Lee G, Dobbs-Dixon I, Mayne N, Amundsen DS, et al. 2016b. The mineral clouds on HD 209458b and HD 189733b. *MNRAS* 460:855–883
- Helling C, Rimmer PB, Rodriguez-Barrera IM, Wood K, Robertson GB, Stark CR. 2016c. Ionisation and discharge in cloud-forming atmospheres of brown dwarfs and extrasolar planets. *Plasma Physics and Controlled Fusion* 58:074003
- Helling C, Vorgul I. 2017. Insight into atmospheres of extrasolar planets through plasma processes. *ArXiv e-prints*
- Helling C, Woitke P, Rimmer PB, Kamp I, Thi WF, Meijerink R. 2014. Disk Evolution, Element Abundances and Cloud Properties of Young Gas Giant Planets. *Life* 4
- Helling C, Woitke P, Thi WF. 2008b. Dust in brown dwarfs and extra-solar planets. I. Chemical composition and spectral appearance of quasi-static cloud layers. *A&A* 485:547–560
- Hellmuth O. 2006. Columnar modelling of nucleation burst evolution in the convective boundary layer - first results from a feasibility study Part I: Modelling approach. *Atmospheric Chemistry & Physics* 6:4175–4214
- Hodosán G, Helling C, Asensio-Torres R, Vorgul I, Rimmer PB. 2016a. Lightning climatology of exoplanets and brown dwarfs guided by Solar system data. *MNRAS* 461:3927–3947
- Hodosán G, Rimmer PB, Helling C. 2016b. Is lightning a possible source of the radio emission on HAT-P-11b? *MNRAS* 461:1222–1226
- Hubeny I. 2017. Model atmospheres of sub-stellar mass objects. *MNRAS* 469:841–869
- Jeong KS, Chang C, Sedlmayr E, Sülzle D. 2000. Electronic structure investigation of neutral titanium oxide molecules Ti_xO_y . *Journal of Physics B Atomic Molecular Physics* 33:3417–3430
- Kataria T, Sing DK, Lewis NK, Visscher C, Showman AP, et al. 2016. The Atmospheric Circulation of a Nine-hot-Jupiter Sample: Probing Circulation and Chemistry over a Wide Phase Space. *ApJ* 821:9
- Kawashima Y, Ikoma M. 2018. Theoretical Transmission Spectra of Exoplanet Atmospheres with Hydrocarbon Haze: Effect of Creation, Growth, and Settling of Haze Particles. I. Model Description and First Results. *ApJ* 853:7
- Keating D, Cowan NB. 2017. Revisiting the Energy Budget of WASP-43b: Enhanced Day-Night Heat Transport. *ApJL* 849:L5
- Knutson HA, Charbonneau D, Allen LE, Fortney JJ, Agol E, et al. 2007. A map of the day-night contrast of the extrasolar planet HD 189733b. *Nature* 447:183–186
- Komacek TD, Showman AP, Tan X. 2017. Atmospheric Circulation of Hot Jupiters: Dayside-Nightside Temperature Differences. II. Comparison with Observations. *ApJ* 835:198
- Kreidberg L, Bean JL, Désert JM, Benneke B, Deming D, et al. 2014. Clouds in the atmosphere of the super-Earth exoplanet GJ1214b. *Nature* 505:69–72
- Krüger D, Sedlmayr E. 1997. Two-fluid models for stationary dust driven winds. II. The grain size distribution in consideration of drift. *A&A* 321:557–567
- Lee G, Dobbs-Dixon I, Helling C, Bogner K, Woitke P. 2016. Dynamic mineral clouds on HD 189733b. I. 3D RHD with kinetic, non-equilibrium cloud formation. *A&A* 594:A48
- Lee G, Helling C, Giles H, Bromley ST. 2015. Dust in brown dwarfs and extra-solar planets. IV. Assessing TiO_2 and SiO nucleation for cloud formation modelling. *A&A* 575:A11
- Lines S, Mayne NJ, Boutle IA, Mannes J, Lee GKH, et al. 2018. Simulating the cloudy atmospheres of HD 209458 b and HD 189733 b with the 3D Met Office Unified Model. *ArXiv e-prints*
- Lothringer JD, Barman T, Koskinen T. 2018. Extremely Irradiated Hot Jupiters: Non-Oxide Inversions, H- Opacity, and Thermal Dissociation of Molecules. *ArXiv e-prints*
- Määttänen A, Montmessin F, Gondet B, Scholten F, Hoffmann H, et al. 2010. Mapping the mesospheric CO_2 clouds on Mars: MEX/OMEGA and MEX/HRSC observations and challenges for atmospheric models. *Icarus* 209:452–469
- Macdonald FA, Wordsworth R. 2017. Initiation of Snowball Earth with volcanic sulfur aerosol

- emissions. *GRL* 44:1938–1946
- Madhusudhan N, Bitsch B, Johansen A, Eriksson L. 2017. Atmospheric signatures of giant exoplanet formation by pebble accretion. *MNRAS* 469:4102–4115
- Mahapatra G, Helling C, Miguel Y. 2017. Cloud formation in metal-rich atmospheres of hot super-Earths like 55 Cnc e and CoRoT7b. *MNRAS* 472:447–464
- Marley MS, Robinson TD. 2015. On the Cool Side: Modeling the Atmospheres of Brown Dwarfs and Giant Planets. *ARA&A* 53:279–323
- Maxted PFL, Anderson DR, Doyle AP, Gillon M, Harrington J, et al. 2013. Spitzer 3.6 and 4.5 μm full-orbit light curves of WASP-18. *MNRAS* 428:2645–2660
- Mayne NJ, Baraffe I, Acreman DM, Smith C, Browning MK, et al. 2014. The unified model, a fully-compressible, non-hydrostatic, deep atmosphere global circulation model, applied to hot Jupiters. ENDGame for a HD 209458b test case. *A&A* 561:A1
- Mendonça JM, Grimm SL, Grosheintz L, Heng K. 2016. THOR: A New and Flexible Global Circulation Model to Explore Planetary Atmospheres. *ApJ* 829:115
- Moses JI, Bézard B, Lellouch E, Gladstone GR, Feuchtgruber H, Allen M. 2000. Photochemistry of Saturn's Atmosphere. I. Hydrocarbon Chemistry and Comparisons with ISO Observations. *Icarus* 143:244–298
- Moses JI, Marley MS, Zahnle K, Line MR, Fortney JJ, et al. 2016. On the Composition of Young, Directly Imaged Giant Planets. *ApJ* 829:66
- Parmentier V, Line MR, Bean JL, Mansfield M, Kreidberg L, et al. 2018. From thermal dissociation to condensation in the atmospheres of ultra hot Jupiters: WASP-121b in context. *ArXiv e-prints*
- Parmentier V, Showman AP, Lian Y. 2013. 3D mixing in hot Jupiters atmospheres. I. Application to the day/night cold trap in HD 209458b. *A&A* 558:A91
- Patzer ABC, Chang C, John M, Bolick U, Sülzle D. 2002. Theoretical study of stationary points of the MgSiO_3 molecule. *Chemical Physics Letters* 363:145–151
- Pérez-Invernón FJ, Luque A, Gordillo-Vázquez FJ. 2017. Three-dimensional modeling of lightning-induced electromagnetic pulses on Venus, Jupiter, and Saturn. *Journal of Geophysical Research (Space Physics)* 122:7636–7653
- Pinhas A, Madhusudhan N, Clarke C. 2016. Efficiency of planetesimal ablation in giant planetary envelopes. *MNRAS* 463:4516–4532
- Plane JMC, Flynn GJ, Määttänen A, Moores JE, Poppe AR, et al. 2018. Impacts of Cosmic Dust on Planetary Atmospheres and Surfaces. *SSRv* 214:23
- Pont F, Sing DK, Gibson NP, Aigrain S, Henry G, Husnoo N. 2013. The prevalence of dust on the exoplanet HD 189733b from Hubble and Spitzer observations. *MNRAS* 432:2917–2944
- Powell D, Zhang X, Gao P, Parmentier V. 2018. Formation of Silicate and Titanium Clouds on Hot Jupiters. *ArXiv e-prints*
- Rietmeijer FJM, III JAN, Karner JM. 1999. Metastable eutectic condensation in a mg-fe-sio-h2-o2 vapor: Analogs to circumstellar dust. *The Astrophysical Journal* 527:395
- Rimmer PB, Helling C. 2013. Ionization in Atmospheres of Brown Dwarfs and Extrasolar Planets. IV. The Effect of Cosmic Rays. *ApJ* 774:108
- Rimmer PB, Helling C. 2016. A Chemical Kinetics Network for Lightning and Life in Planetary Atmospheres. *ApJS* 224:9
- Rimmer PB, Helling C, Bilger C. 2014. The influence of galactic cosmic rays on ion-neutral hydrocarbon chemistry in the upper atmospheres of free-floating exoplanets. *International Journal of Astrobiology* 13:173–181
- Rodriguez-Barrera MI, Helling C, Wood K. 2018. Environmental effects on the ionization of brown dwarf atmospheres. *ArXiv e-prints*
- Sabri T, Gavilan L, Jäger C, Lemaire JL, Vidali G, et al. 2014. Interstellar Silicate Analogs for Grain-surface Reaction Experiments: Gas-phase Condensation and Characterization of the Silicate Dust Grains. *ApJ* 780:180
- Sagan C, Khare BN. 1979. Tholins - Organic chemistry of interstellar grains and gas. *Nature*

- Santos NC, Adibekyan V, Dorn C, Mordasini C, Noack L, et al. 2017. Constraining planet structure and composition from stellar chemistry: trends in different stellar populations. *A&A* 608:A94
- Schellart P, Trinh TNG, Buitink S, Corstanje A, Enriquez JE, et al. 2015. Probing Atmospheric Electric Fields in Thunderstorms through Radio Emission from Cosmic-Ray-Induced Air Showers. *Physical Review Letters* 114:165001
- Showman AP, Cooper CS, Fortney JJ, Marley MS. 2008. Atmospheric Circulation of Hot Jupiters: Three-dimensional Circulation Models of HD 209458b and HD 189733b with Simplified Forcing. *ApJ* 682:559–576
- Smith RNB. 1990. A scheme for predicting layer clouds and their water content in a general circulation model. *Quarterly Journal of the Royal Meteorological Society* 116:435–460
- Snellen IAG, de Kok RJ, le Poole R, Brogi M, Birkby J. 2013. Finding Extraterrestrial Life Using Ground-based High-dispersion Spectroscopy. *ApJ* 764:182
- Trinh TNG, Scholten O, Bonardi A, Buitink S, Corstanje A, et al. 2017. Thunderstorm electric fields probed by extensive air showers through their polarized radio emission. *PhRvD* 95:083004
- Vorgul I, Helling C. 2016. Flash ionization signature in coherent cyclotron emission from brown dwarfs. *MNRAS* 458:1041–1056
- Woitke P, Helling C. 2003. Dust in brown dwarfs. II. The coupled problem of dust formation and sedimentation. *A&A* 399:297–313
- Woitke P, Helling C, Hunter GH, Millard JD, Turner GE, et al. 2017. Equilibrium chemistry down to 100 K - Impact of silicates and phyllosilicates on carbon/oxygen ratio. *ArXiv e-prints*
- Wong I, Knutson HA, Kataria T, Lewis NK, Burrows A, et al. 2016. 3.6 and 4.5 μm Spitzer Phase Curves of the Highly Irradiated Hot Jupiters WASP-19b and HAT-P-7b. *ApJ* 823:122
- Wong I, Knutson HA, Lewis NK, Kataria T, Burrows A, et al. 2015. 3.6 and 4.5 μm Phase Curves of the Highly Irradiated Eccentric Hot Jupiter WASP-14b. *ApJ* 811:122
- Zellem RT, Lewis NK, Knutson HA, Griffith CA, Showman AP, et al. 2014. The 4.5 μm Full-orbit Phase Curve of the Hot Jupiter HD 209458b. *ApJ* 790:53
- Zhang X, Showman AP. 2018. Global-Mean Vertical Tracer Mixing in Planetary Atmospheres. *ArXiv e-prints*